J Mater Sci (2008) 43:5654–5658
DOI 10.1007/s10853-008-2759-y

LETTER

Microstructural characterization of Hadfield austenitic manganese steel

Ashok Kumar Srivastava · Karabi Das

Received: 21 January 2008 / Accepted: 28 May 2008 / Published online: 10 June 2008

Hadfield austenitic manganese steels are ferrous alloys containing approximately 1.0–1.4% C and 10–14% Mn in a 1:10 ratio [1]. It exhibits high toughness, high ductility, high work hardening ability and excellent wear resistance. Because of the excellent combination of these properties this steel has been accepted as a very useful engineering material. It is broadly used in the fields of earthmoving, mining, quarrying, oil well drilling, steelmaking, railroading, dredging, naval, lumbering excavators, and mineral crushing equipment [2–5].

Hadfield austenitic manganese steel in the as-cast condition contains $(Fe, Mn)_3C$ carbides. It is a common industrial practice to solutionize the material before use so that $(Fe, Mn)_3C$ goes into solution giving completely austenitic structure. Generally, it is solution-annealed at 1,050 °C for few hours followed by water quenching. In the absence of an inert atmosphere, the high solutionizing temperature normally produces considerable surface decarburization and the loss of manganese leading to the formation of α-martensite on the surface layer upon quenching [6–8]. It work-hardens very rapidly upon plastic deformation. In earlier studies, it is reported that the strain hardening in this steel is caused by the strain-induced transformation of γ to α or ε-martensites [9–11]. Smith et al. [12] have reported that the strain-induced transformation is occurring only due to decarburization or local segregation of manganese leading to unstable austenite composition.

It has been reported in the literature that elaborate heat-treatment cycles are necessary to optimize the form and distribution of the precipitate in the modified Hadfield austenitic manganese steels [12–18]. However, the associated decarburization with the heat-treatment has not been reported. In the present investigation, an effective solution heat-treatment has been adopted to dissolve the $(Fe, Mn)_3C$ carbides in Hadfield austenitic manganese steel. The influence of the solution annealing heat-treatment on the microstructure, hardness values and abrasive wear resistance of Hadfield austenitic manganese steel have been also discussed.

The synthesis of the steel was carried out in a high frequency air induction furnace. At first the blend of steel scrap (0.049%C, 0.43%Mn, 0.028%Si, 0.023%P, 0.013%S, 0.003%Al, 0.035%Cr and balance Fe, all in wt.%) and cast iron (4.5%C, 0.043%Mn, 1.05%Si, 0.175%P, 0.043%S and balance Fe, all in wt.%) was heated to 1,580 °C and maintained at that temperature for 15 min followed by addition of calculated amount of electrolytic manganese (95% purity) to the melt. The melt was stirred continuously at this temperature for 10 min and finally cast in a metallic mould.

The chemical compositions of Hadfield austenitic manganese steel, steel scrap and cast iron were determined by means of omission electron spectroscope (OES) and carbon/sulphur analyzer. Specimens of dimension 12 mm × 12 mm × 10 mm for metallography were sectioned from the cast material and polished according to the standard metallographic technique. A 2% nital (2 mL HNO_3 + 98 mL ethanol) solution was used as an etchant to reveal microstructures. The microstructures of the as-cast and solution annealed specimens were subsequently characterized using an optical microscope (OM), a scanning electron microscope (SEM) and X-ray diffractometer (XRD) using CoK_α radiation. The Thermo-Calc software was used to plot the phase diagram using TCFE3 database.

A. K. Srivastava · K. Das (✉)
Department of Metallurgical and Materials Engineering,
Indian Institute of Technology, Kharagpur 721302, India
e-mail: karabi@metal.iitkgp.ernet.in

The Vickers scale using diamond indentor and 50-g load for 20 s of time was used to measure the micro-hardness. Abrasive wear tests were carried out against 220 grit SiC paper affixed to a rotating flat disc of 250 mm diameter. The rotating speed and the track diameter were fixed as 300 r.p.m. and 100 mm, respectively. The experiments were carried out at the load of 14.7 and 24.5 N. Wear rate of the specimens has been computed by the weight loss technique. The weight loss has been converted to volume loss and then wear data have been plotted as cumulative volume loss as a function of sliding distance.

Figure 1a and b show the as-cast microstructure of Hadfield austenitic manganese steel in which the (Fe, $Mn)_3C$ carbides are precipitated along the austenite grain boundaries. The formation of (Fe, $Mn)_3C$ carbides along the austenite grain boundaries leads to the depletion of carbon and manganese in the matrix adjacent to the carbide network. Since carbon and manganese are austenite stabilizers, the depletion of carbon and manganese causes austenite matrix to be unstable leading to the decomposition of the austenite matrix to α-ferrite and (Fe, $Mn)_3C$ carbides. Figure 1b shows a higher magnification SEM micrograph focusing on a carbide network. It reveals that an alternative lamellae of α-ferrite and (Fe, $Mn)_3C$ carbides forms adjacent to the carbide network. The x-ray diffraction pattern (Fig. 1c) confirms that the microstructure consists of austenite, α-ferrite and (Fe, $Mn)_3C$ carbides. Dissolution of this (Fe, $Mn)_3C$ carbide is the primary reason of heat-treatment of austenitic manganese steel.

It has been observed from the SEM micrograph (Fig. 2a) of solution-annealed specimen that α-martensite forms on the surface of the specimen. The XRD (Fig. 2c) from the surface shows the presence of α-martensite and (Fe, $Mn)_3C$ carbides. In the absence of an inert atmosphere, the loss of carbon and manganese from the surface causes the formation of a thin layer of α-martensite on the surface of the material during water quenching. The optical micrograph (Fig. 2b) of the solution-annealed specimen after removing the decarburized layer from the surface shows that most of the (Fe, $Mn)_3C$ carbides, present along the austenite grain boundaries, are dissolved. The XRD pattern (Fig. 2d) confirms that the matrix attains completely austenitic structure with small amount of (Fe, $Mn)_3C$ carbides. The negative effects of the carbide network can be avoided by solution annealing treatment. However, solution annealing at this temperature coarsens the austenite grains which can be clearly seen in Fig. 2b. In the selection of a suitable solution annealing temperature, huge care must be taken to avoid the excessive coarsening of austenite grains.

A vertical section of the Fe–C–Mn phase diagram is shown in Fig. 3a, which has been plotted with the help of thermo-calc software. The evaluated values of Ac_1 and Ac_3 temperatures are 651 and 983 °C, respectively. The solution annealing temperature has been chosen as 1100 °C

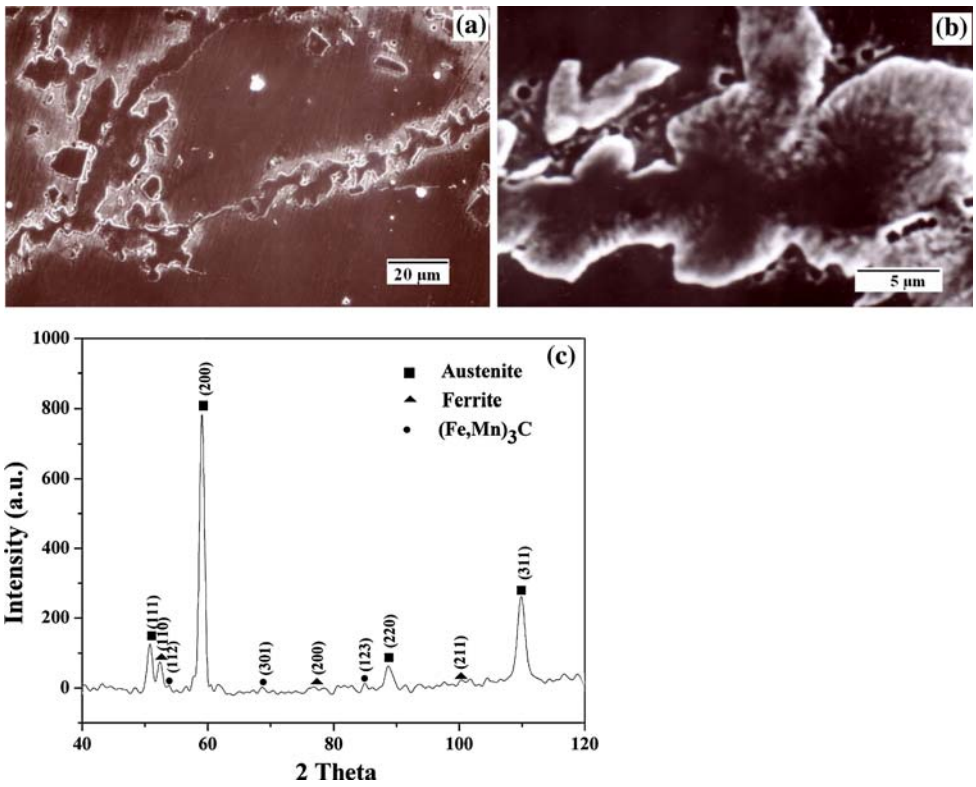

Fig. 1 SEM micrographs at (**a**) low and (**b**) high magnification and (**c**) XRD of as-cast Hadfield austenitic manganese steel

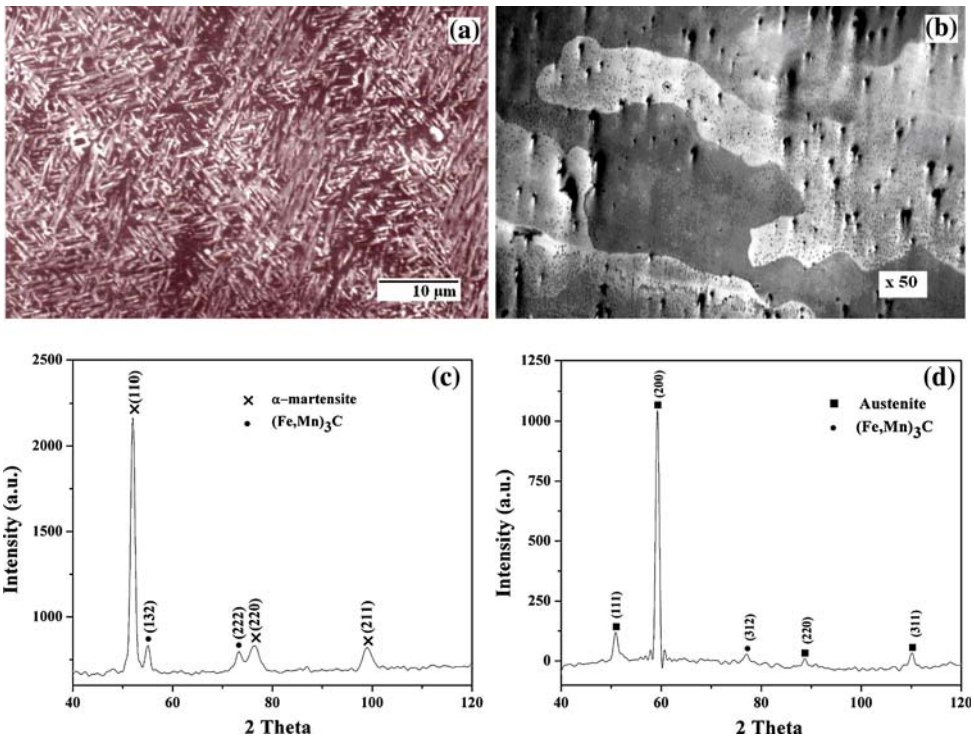

Fig. 2 SEM micrographs from (**a**) the surface and (**b**) the core and XRD from (**c**) the surface and (**d**) the core of the solution-annealed Hadfield manganese steel

with the help of the calculated phase diagram by keeping an aim to get a completely austenitic single phase structure. A micro-hardness profile across the length of the specimen is shown in Fig. 3b. It is found that the hardness values up to 1 mm of depth are almost the same due to the formation of hard α-martensite phase. In the material under investigation the thickness of the decarburized layer is of the order of about 1–2 mm. From 3 to 9 mm of distance from the surface layer, the hardness values remain almost constant due to the formation of completely austenitic matrix with marginal amount of (Fe, Mn)$_3$C carbide in the core. The hardness profile confirms the formation of α-martensites on the surface and the austenite in the core region.

Figure 4a and b shows the variation of cumulative volume loss and wear rate with sliding distance for as-cast austenitic manganese steel. It is clear that both cumulative volume loss and wear rate increases with the load. At higher load, the depth of penetration of SiC abrasive increases and hence material removal is more. Figure 4b shows that at both applied loads, the wear rate is more at the initial stage and then almost levels off with further increasing sliding distance. This is due to the fact that initially SiC abrasive particles remove the material from soft austenitic manganese steel matrix. The hardness of the surface increases during wear testing since austenitic manganese steel has substantial work hardening capacity resulting in a decrease in wear rate at large sliding distance. Figure 4c and d show the SEM micrographs of the worn surface of the steel tested under the applied loads of 14.7 and 24.5 N, respectively. The worn surface has been

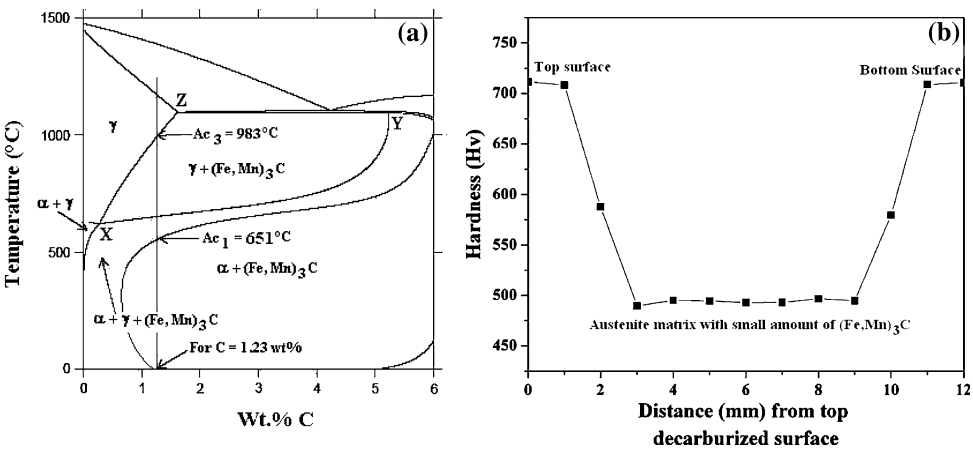

Fig. 3 (**a**) Pseudo-ternary phase diagram of Hadfield manganese steel under investigation and (**b**) Micro-hardness profile of solution-annealed specimen

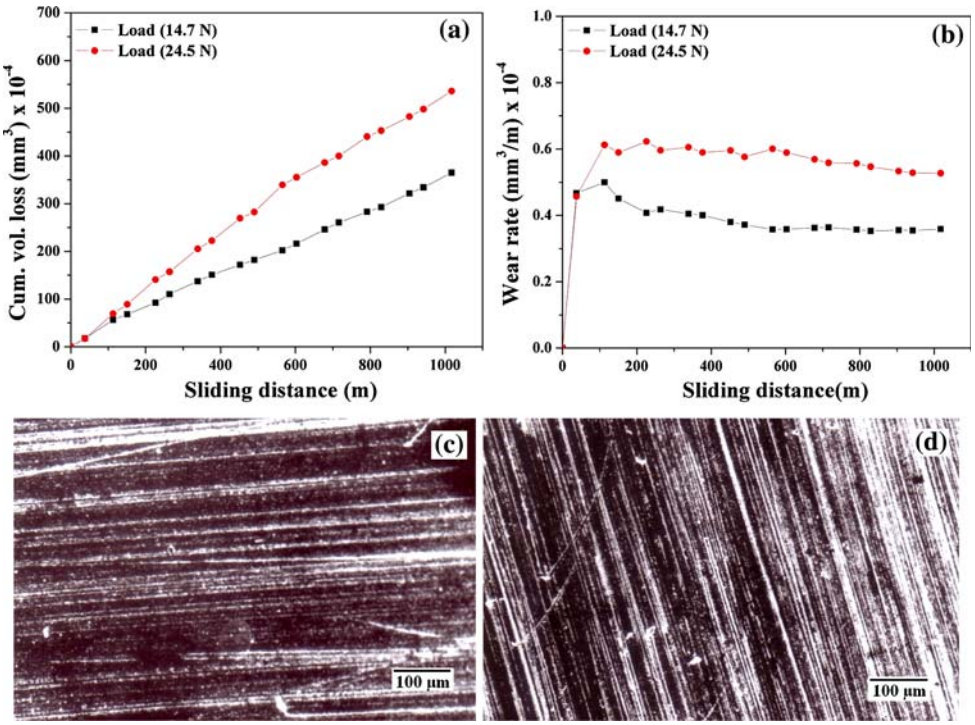

Fig. 4 (**a**) Cumulative volume loss and (**b**) wear rate and SEM micrographs of the worn surface at the loads of (**c**) 14.7 and (**d**) 24.5 N of as-cast Hadfield austenitic manganese steel

characterized by long continuous grooves, which forms as the SiC abrasive particles plough across the surface. The severity of the indentation of the abrasive particles is substantially more at the load of 24.5 N (Fig. 4d) compared to 14.7 N. Hence, the depth of grove is more at 24.5 N load compared to that at 14.7 N load.

A comparison of the cumulative volume loss and the wear rate with sliding distance for as-cast and solution-annealed (with and without the removal of surface layer) specimens are shown in Fig. 5. It has been observed from Fig. 5a that the cumulative volume loss is maximum in the case of as-cast austenitic manganese steel and minimum in the case of solution-annealed specimen after removing the surface layer. The solution annealing treatment improves the strength and toughness of the austenitic manganese steel matrix by dissolving $(Fe, Mn)_3C$ carbides. The abrasive wear resistance of Hadfield austenitic manganese steel increases with the solubility of the carbides [19]. Hence, the solution-annealed specimen after removing the surface layer exhibits best abrasive wear resistance among the tested materials.

The solution-annealed specimen with surface layer consists of α-martensite on the surface. However, the core remains austenitic which has substantial work-hardening

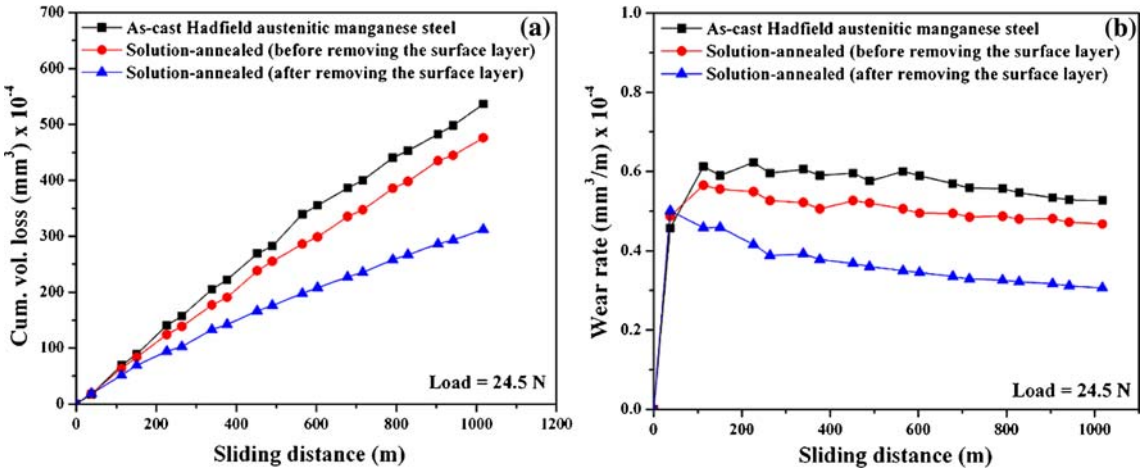

Fig. 5 (**a**) Cumulative volume loss and (**b**) wear rate of as-cast and solution-annealed (before and after removing the surface layer) specimen at the load of 24.5 N

capacity. Hence, its abrasive wear resistance is better than the as-cast material. Figure 5b shows that the wear rate of all the materials is more at the initial stage and then decreases slightly and finally levels off with the increase in sliding distance. A strong work-hardening layer with high hardness develops on the friction surface resulting in improvement in the abrasive wear resistance.

To summarize, the $(Fe, Mn)_3C$ carbides and α-ferrite form an alternative lamellae adjacent to the carbides network in the as-cast microstructure. It should not be heat-treated in open-air or a weakly oxidizing atmosphere unless the decarburized layer is removed before any testing or use. The heat-treatment temperature and time should be optimized for attaining the completely austenitic structure and at the same time avoid excessive grain growth. The SEM, XRD and micro-hardness profile clearly indicate that the surface and core of solution-annealed specimen consist of mainly α-martensite and austenite, respectively. The abrasive wear resistance is more at the lower load. The solution-annealed specimen after removing the surface layer shows the best abrasive wear resistance.

Acknowledgement The authors wish to acknowledge Naval Research Board, New Delhi, India, for sponsoring this research work.

References

1. Curiel-Reyna E, Contreras J, Rangel-Ortis T, Herrera A, Baños L, del Real A, Rodríguez ME (2008) Mater Manuf Process 23:14–20. doi:10.1080/10426910701524352
2. Roberts WN (1964) Trans Metall Soc AIME 230:372–373
3. Dastur YN, Leslie WC (1981) Metall Trans 12A:749–759
4. Adler PH, Olson GB, Owen WS (1986) Metall Trans 17A:1725
5. Owen WS, Grujicic M (1998) Acta Mater 47:111. doi:10.1016/S1359-6454(98)00347-4
6. White C, Honeycombe RWK (1962) JLSL 200:457
7. Sant SB, Smith RW (1985) In: Proceedings of the conference on strength of metals and alloys, vol 1. Pergamon Press, Montreal, Canada, p 219
8. Sant SB, Smith RW (1987) J Mater Sci 22:1808–1814. doi:10.1007/BF01132410
9. Xie JP, He ZM, Fu SB, Jiang QQ (1990) Materialwiss Werkst 21:287. doi:10.1002/mawe.19900210709
10. Efros B, Beygelzimer Y, Deryagin A, Efros N, Pilyugin V, Orlov D (2004) Ultrafine Grained Mater III:401
11. Wang TS, Lu B, Zhang M, Hou RJ, Zhang FC (2007) Mater Sci Eng A 458:249–252. doi:10.1016/j.msea.2006.12.066
12. Smith RW, DeMonte A, Mackay WBF (2004) J Mater Process Tech 153–154:589–595. doi:10.1016/j.jmatprotec.2004.04.136
13. Middleham TH (1964) Alloys Metab Rev 12(112):11
14. Grigorkin VI, Korotushenko GV (1968) Metab Sci Heat Treat Metab 2:130–132. doi:10.1007/BF00657754
15. Grigorkin VI, Frantsenyuk IV, Galkin IP, Osetrov AA, Chemeris AT, Chernenilov MF (1974) Metab Sci Heat Treat Metab 16(4):52–354
16. Sil'man GI, Pristuplyuk NI, Frol'tsov MS (1980) Metab Sci Heat Treat Metab 22(2):124–127. doi:10.1007/BF00699676
17. Richardson DC, Mackay WBF, Smith RW (1981) Solidification Technology. The Metals Society, Warwick, England, pp 409–413
18. Norman TE, Doane DV, Soloman A (1960) AFS Trans 68:287–300
19. Ksenofontov VP (1967) Translated from *Metallovedenie i Termicheskaya Obrabotka Metallov* 9:73